JMEPEG (2021) 30:546–555
https://doi.org/10.1007/s11665-020-05332-5

1059-9495/$19.00

Effect of Aging Temperature on the Microstructure, Local Mechanical Properties, and Wear Behavior of a UNS S32750 Super Duplex Stainless Steel

Bouzid Maamache, Billel Cheniti, Brahim Belkessa, Karima Tahar-chaouch, and Ramdhane Kouba

Submitted: 2 September 2020 / Revised: 28 October 2020 / Accepted: 1 November 2020 / Published online: 23 November 2020

In this paper, the effect of aging temperature on the microstructure, local mechanical properties and wear behavior of a UNS S32750 super duplex stainless steel is investigated. A massive preferential precipitation of σ phase and Cr_2N is detected at the periphery of ferrite with an increase in their extent as aging temperature increases. Simultaneously, the δ phase decomposition is accentuated with temperature and reaches its maximum at 850 °C. This behavior results in an enhancement in hardness and Young's modulus accompanied by a higher plasticity ratio. The wear resistance of the aged samples is investigated in terms of friction coefficients and wear rates against two counterparts. The wear performance follows σ phase presence, the higher σ phase extent, the higher the wear resistance. It is found that the change in wear mechanisms in the 850 °C aged samples from abrasive against AISI-304L counterpart to adhesive-oxidative against Al_2O_3 counterpart is responsible in the increase in wear resistance.

Keywords 2507 SDSS, aging temperature, microstructure, nano-indentation, precipitates, wear resistance

1. Introduction

Super duplex stainless steels (SDSSs) with dual-phase ferrite–austenite microstructure have raised much interest as structural materials in research and industrial fields (Ref 1). Thanks to their attractive mechanical properties, (high hardness, strength and ductility) and good resistance to the local pitting and stress cracking corrosion, especially in chloride environment (Ref 2, 3), SDSSs are widely designed as a solution in the marine, electrochemical industries and lightweight structures (Ref 4). Nevertheless, the above outstanding properties are strongly dependent on the manufacturing processes and the thermal history of the SDSS materials (Ref 5). It is well-known that annealing treatment of 2507 SDSS at temperature bellow 1000 °C leads to the phase decomposition of ferrite phase (δ) to sigma (σ) phase and carbides which results in the increase in Ni concentration in the surrounding material, consequently, the formation of secondary austenite (γ_2) (Ref 6). These precipitates deteriorate the toughness of the SDSS and decrease its corrosion performance by stimulating local corrosion attack around the precipitates already formed (Ref 5). Nilsson (Ref 7) highlighted that at temperature range between 600 and 1000 °C, close-packed brittle precipitate, e.g., σ phase is mostly formed. Vahid et al. (Ref 5) reported that the precipitation of only 5% of σ phase breaks down drastically the mechanical properties of the SDSS to 80% and the corrosion resistance to 25% (Ref 8). The thermodynamic instability of the δ in 2507 SDSS in the temperature range mentioned above is deeply investigated in literature, where the phase proportions changes as exposure time of the SDSS at determined temperature increases (Ref 9, 10). Mahesh et al. (Ref 9) studied the effect of heat treatment on the mechanical properties and wear resistance of 2507 treated at 850 °C for 1 h. They found that the precipitation of σ phase with high Cr-content in the ferrite particles caused an increase in the hardness and wear resistance of the treated material. Similar results were found by Marques et al. (Ref 7) where an interesting decrease in abrasive wear coefficient of about 50% of the sample heat treated at 850 °C was observed. This behavior is attributed to the hardening effect induced by the precipitation of ternary phases (α', σ and chi 'χ') as a result of δ phase decomposition at high temperatures (478, 850 and 950 °C) where an excessive dissolution of ferrite and the formation of undesirable precipitates worsen the ductility of the 2507 SDSS (Ref 11). In other research work, the tribological behavior of a fritted 2507 SDSS at elevated temperature under different applied loads was investigated by Wand et al. (Ref 12). They revealed formation of oxide layers (Fe_2O_3 and Fe_3O_4) and surface softening as the working temperature increased to 400 °C. Furthermore, the wear rate was simultaneously controlled by the interrelated effect of applied load and working temperature. Numerous research works studied the effect of aging treatment on the kinetics of sigma phase precipitation and macro-mechanical properties of 2507 SDSS (Ref 2, 7, 9, 13). However, few works employed nano-indentation technique to investigate the local mechanical properties of the 2507 on the precipitate level (Ref 14). Hence, it is necessary to point out the nano-mechanical properties of sigma phase and their effect of the macro-mechanical behavior and wear performance of the 2507 SDSS subjected to several aging treatments.

Bouzid Maamache, Billel Cheniti, and **Brahim Belkessa**, Research Center, Industrial Technologies CRTI, P.O. Box 64, Chéraga, Algeria; **Karima Tahar-chaouch**, Département de mécanique Faculté de Technologies, Université Blida 1, BP 270 route de Soumaa Blida, Blida, Algeria; and **Ramdhane Kouba**, Laboratoire de Technologie des Matériaux, Département SDM, Facultéde Génie Mécanique et Génie des Procédés, USTHB, BP 32 El-Alia, 16111 Alger, Algeria. Contact e-mail: maamache2002@yahoo.fr.

Generally, in nuclear and chemical industries, 2507 SDSSs are usually used and exposed to high service temperature, where at specific exposition time, sigma phase, carbides and secondary phases start to precipitate massively, which alter significantly the mechanical behavior and the wear resistance. However, the literature reported limited studies of the sliding wear behavior of 2507 SDSS at elevated temperature. Therefore, and taking into account the thermal cycle of the 2507 SDSS adopted in electrochemical industries, the present work aims to study the influence of phase precipitations on the microstructure and mechanical properties of the 2507 SDSS subjected to several aging temperatures (600-1050 °C). The influence of aging temperature on the dry tribological behavior and wear mechanisms of the 2507 SDSS under Al_2O_3 and AISI 304L counterparts are also investigated.

2. Materials and Experimental Procedures

The investigated material is a UNS S32750 super duplex stainless steel (2507 SDSS) received in pipe form of 160 mm diameter and 7 mm thick with the chemical composition as given in Table 1. Solution treatment at 1200 °C is performed for 1 h holding time followed by water quenching. Subsequently, several aging treatments are carried out for the temperature range 650-1050 °C and that for 1 h holding time. Thereafter, the obtained samples are polished using standard techniques of mechanical polishing then electrolytically etched using LectroPol-5 machine with 1 M KOH solution working at 5 V for 6 s. Microstructure examination is conducted using Nikon optical microscope and a ZEISS Gemini SEM 300 scanning electron microscope (SEM) equipped with energy-dispersive spectroscopy (EDS) detector for the chemical analysis of the different constituents. Phase's fraction of the samples issued from different aging temperatures is measured through automatic image analysis using Image-J software. X-ray diffraction (XRD) analysis is performed to identify the phases obtained from each aging temperature using Bruker D2 Phaser 2nd generation with Cu (Kα) radiation (0.15406 nm) operating at 40 kV and 40 mA. The obtained patterns are characterized by HighScore software using PDF4 database.

The local mechanical properties of the different phases are evaluated through nano-indentation measurements using Anton-Paar NHT-3 nanoindenter with a Berkovich tip under a 20 mN applied load. The tests are conducted in each selected phase that includes ferrite phase, austenite phase and sigma phase. Hardness H_{IT} and Young' modulus E_{IT} values are calculated using the Oliver and Pharr method (Ref 15) for an average value of 3 indent tests. On the other side, the ratio of hardness (H_{IT}) and Young's modulus (E_{IT}) is calculated to evaluate the strain to failure so-called plasticity index of the aged materials, in order to predict their wear behavior.

The wear behavior of the as-annealed (solution treated at 1200 °C) and aged samples is investigated through oscillating sliding test using ball-on disk tribometer (CSM Instruments Inc-Peseux, Switzerland) and TriboX software, under dry conditions at room temperature. The tests are performed using two types of counterpart with 6 mm diameter: (1) alumina (Al_2O_3) ball with 16.1 GPa of hardness and 256 nm of root mean square (RMS) and (2) AISI 304L stainless steel ball (3 GPa and 220 nm of hardness and RMS, respectively). The AISI 304L austenitic stainless steel has lower hardness than the 2507 SDSS one, hence adhesion is expected during the tests. However, the Al_2O_3 ball with high hardness is quiet suitable to test and compare the wear behavior of the treated samples under these two different conditions. During the tests, 10 N applied load is selected for 200 m sliding distance and 5 sliding amplitude. The working parameters are summarized in Table 2. The wear rates (W) is calculated using Eq 1, and the width of the wear tracks is measured using 2D profilometer software

$$W = V/d_S F \quad \text{(Eq 1)}$$

where V is the volume loss, d_s is the sliding distance (m), and F is the applied load (N).

3. Results and Discussion

3.1 Effect of Aging Temperature on the Microstructural Evolution

Figure 1(a), (b), (c), (d), (e), and (f) shows the optical micrographs of the as-annealed sample microstructure and those obtained from different aging temperatures. It can be seen in the as-annealed sample (Fig. 1a) an elongated microstructure of the γ phase (bright phase) embedded in the continuous δ matrix (dark phase) along the rolling direction, without apparent precipitations or secondary phases. The volume fraction of both phases calculated using Image-J software is found to be 48 and 52% for γ and δ phase, respectively. Several research works reported that sigma (σ), Chi (χ) and secondary phases start to precipitate at temperatures below 650 °C (Ref 3, 16, 17). In the present work, precipitation of secondary phases in the sample aged at 650 °C are barely detected in double and triple junctions of δ phase, due to their small extents (small dark spots), (Fig. 1b). The precipitates amount is related to their transformation kinetic that is strongly affected by the exposure time at the determined temperature, where 1 h allows only the formation of small amount of precipitates. Nevertheless, remarkable precipitates nucleate at the periphery of δ phase and at δ/γ interface in the sample aged at 750 °C (Fig. 1c) and grow into the δ phase as shown in Fig. 2(a), which indicates the sensitivity of the SDSS to χ and σ phases' precipitation at this temperature. The volume fraction of σ phase at 750 °C aging temperature is about 5% and that of χ phases is 8%. As the temperature is increased to 850 °C, these amounts increase gradually and reach their maximum values of 17% and 11% for σ and χ phases, respectively, as shown in Fig. 1(d). The nucleation of σ phase is generally accompanied by carbides and

Table 1 Chemical composition of the UNS S32750 used

Elements, wt.%	C	Cr	Fe	Ni	Mo	Mn	N	V	Al	S	Si	Ti
UNS S32750	0.033	**26.5**	61.3	**6.63**	**3.51**	0.791	**0.236**	0.174	0.013	0.014	0.445	0.006

Bold values are the most influential alloying elements in the SDSS used

secondary austenite (γ_2) formation with a small needle shape (Widmannstätten) of the later as a result of δ phase decomposition ($\delta \rightarrow \sigma + \gamma_2$). At elevated aging temperatures (950 °C), the extent of δ phase increases and keeps that trend up to 1050 °C aging temperature as illustrated in Fig. 1(e) and (f), respectively. As the temperature is increased (750-850 °C), the N extent in the ferrite increased. In hors equilibrium conditions, i.e., during rapid cooling, N exceeds the solubility limit in ferrite and forms with chromium nitrides as Cr_2Nin the δ matrix (Ref 18). At 850 °C (Fig. 2b) Cr_2N, σ phase, χ phase and austenite are the only stable phases at this temperature, where δ phase is thermodynamically instable and will gradually transform to the equilibrium phases in an adequate time as indicated in TTT diagram of the 2507 SDSS (Ref 7). Kinetics of precipitation in 2507 SDSS for long period holding time is investigated in literature (Ref 7, 18). It was found the precipitation of sigma and nitrides after few minutes at 850 °C as a result of the eutectoid decomposition of ferrite (Ref 16). At this temperature, the decomposition of ferrite continuous until its complete disappearance if sufficient time is allowed. However, it is found, in the present work, that after 1 h holding time, the dissolution of ferrite is not complete and the volume fraction of σ phase, χ phase, γ_2 and nitrides increases to the detriment of δ phase with increasing aging temperature until its maximum at 850 °C resulting in considerable residual amount of ferrite. The concentration of the

Table 2 Wear test parameters

Applied load, N	10
Balls	Alumina AL_2O_3 AISI 304L
Balls diameter, mm	6.35
Roughness of the sample surface, µm	0.01
Sliding distance, m	200
Sliding amplitude, mm	5
Linear velocity, m/s	0.048
Temperature, °C	26 ± 2
Humidity, %	45 ± 4

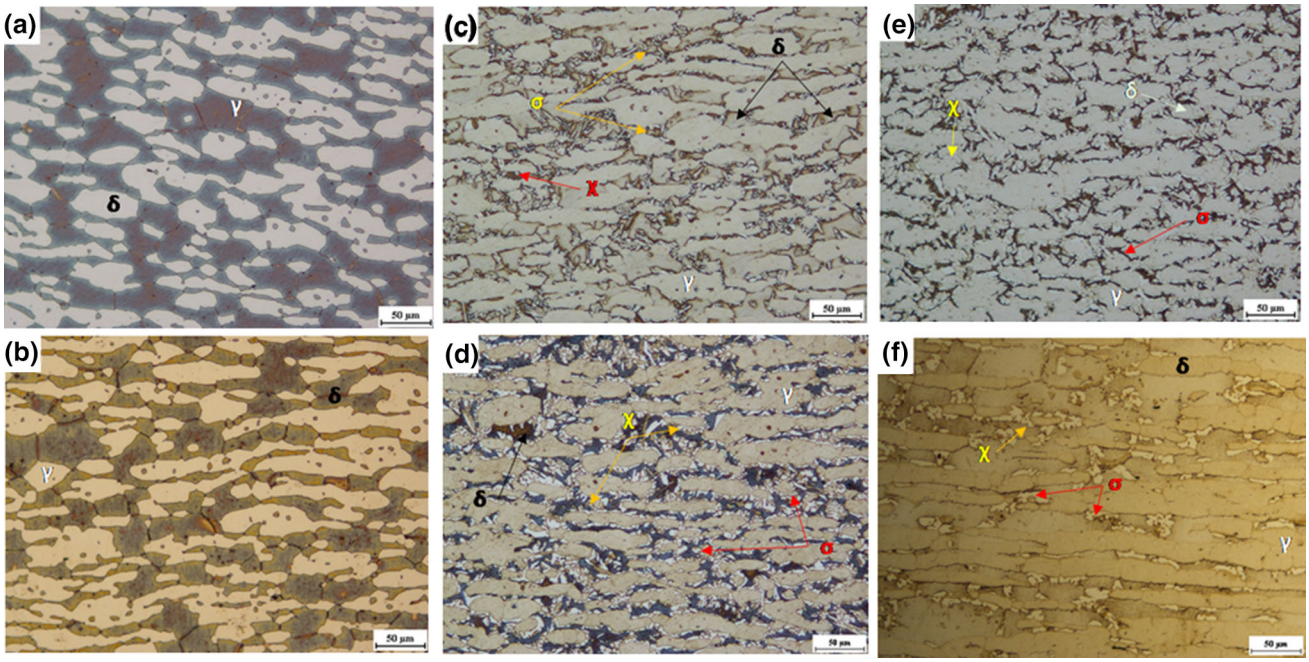

Fig. 1 Optical micrographs of UNS S32750 microstructure of (a) as-annealed specimen and aged at (b) 650 °C, (c) 750 °C, (d) 850 °C, (e) 950 °C and (f) 1050 °C

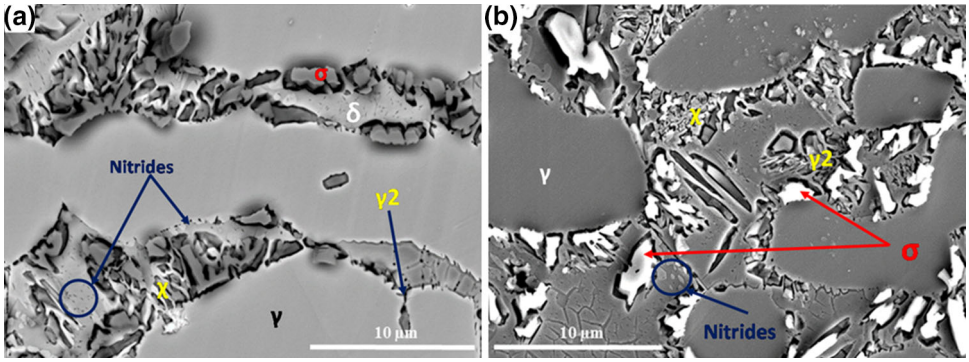

Fig. 2 SEM microstructure images of UNS S32750 samples aged (a) at 750 °C and (b) at 850 °C

major constituted elements of δ phase, i.e., Cr and Mo elements is strongly decreased and the Cr content goes below 12 wt.% (Spot 2 in Fig. 3) which with high extent of Ni allows the formation γ_2 at the surrounding of ferrite phase as a result its decomposition. The decrease in Cr content ($\sim$ 3 wt.%) is far to be sufficient to ensure the passive protection of δ phase, resulting in the creation of Cr-depletion region susceptible to corrosion (Ref 19).

The EDS point analysis shown in Fig. 3 reveals a high concentration of Cr and Mo element in the white phases (Spot 3) in the surrounding of δ phase and the δ/γ boundaries which corresponds to σ phase, while χ phase is present as a distinct white needles (Spot 1) with high Cr $\sim$ 30 and $\sim$ 5 wt.% Mo constituents. The high concentration of N element ($\sim$ 16 wt.%) in Spot 4 in Fig. 3 suggests the presence of nitrides clusters, randomly present in/and around δ phase.

The evolution of different phases with aging temperature is in good agreement with the results of their volume fractions calculated by Thermo-calc software (Fig. 4). Nevertheless, the amounts of these fractions are much higher compared to the results obtained using image treatment (image-J software). This difference is more probably related to (1) the images quality and the electrochemical etching that may hide some parts of the phases to be calculated and (2) Thermo-calc software calculation that does not take in consideration the kinetic of transformation (time), where the 1 h holding time is insufficient for the complete decomposition of δ phase and the formation of stable phases.

X-ray diffraction spectra of the as-annealed and the samples aged at different temperatures are illustrated in Fig. 5. It can be seen that only δ and γ peaks are present in the as-annealed sample diffractogram, where δ peak appears to be more intense relative to γ phase. This indicates that no sigma phase, carbides or secondary phases are precipitated in this condition. Similar results are found in the sample aged at 650 °C, where the intensity peak of δ phase is slightly decreased which confirms the formation and presence of very low volume fraction of secondary phases that are below the detectability limit of the XRD and/or SEM employed. It is seen from the diffractogram of the samples aged at 850 °C that the peak of δ phase is remarkably reduced, which is related to its low volume fraction due to its decomposition and formation of Cr_2N with σ phase. While at 950 °C, the δ phase peak is more intense but less than the one in the as-annealed sample because of eutectoid transformation of δ into σ as well as Cr_2N.

3.2 Effect of Aging on the Local Mechanical Properties of Different Phases

Figure 6(a) shows the load–displacement curves of ferrite, austenite and sigma phases of the sample aged at 750 °C. The corresponding hardness (H_{IT}) and elastic modulus (E_{IT}) values for each phase are summarized in Table 3. As seen, the maximum penetration depth is greater in the austenite phase than that in ferrite, while sigma phase exhibits reduced penetration, indicating that the latter is the harder phase. Furthermore, in the unloading segment of the curves, the slope is steep in σ phase than that in the other phases, suggesting its higher stiffness value. In the most often cases, the hard phases demonstrates high Young's modulus (Ref 20), as for σ phase (8.8 and 250 GPa for H_{IT} and E_{IT}, respectively), whereas the lowest values are recorded in austenite with 5.9 and 230 GPa for H_{IT} and E_{IT}, respectively. These values are in coherence with those obtained by Argandoña et al. (Ref 14) and significantly higher than those presented by previous research works (Ref 21, 22). The main reason to this difference can be attributed, on the one hand, to the indentation size effect (ISE), i.e., the higher the applied load, the lower the hardness; and, on the other hand, to the surface characteristics (scratches, oxides,…) and the emplacement of the indentation into the microstructure (grain boundary) that may strongly influence the measurements (Ref 23). As discussed in section 3.1, the volume fraction of δ and σ phases changes with annealing temperatures. Knowing the hardness and elastic modulus of each phase with their respective volume fractions, the global

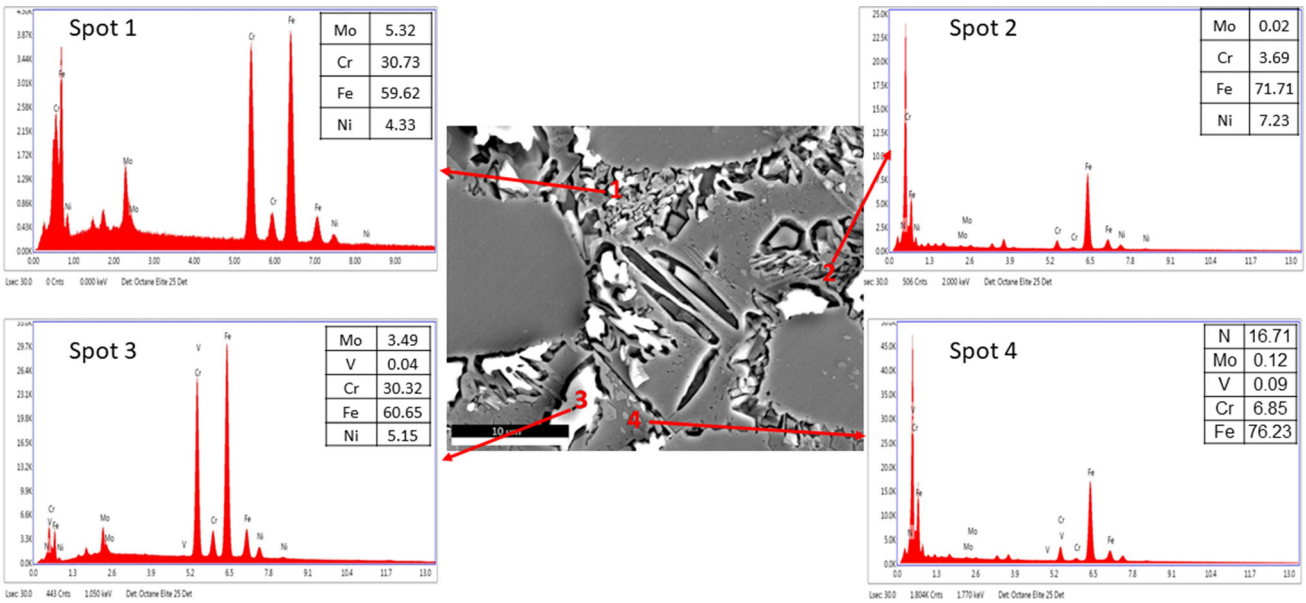

Fig. 3 Microstructure of the sample aged at 850 °C with the corresponding EDS point analysis conducted in different regions

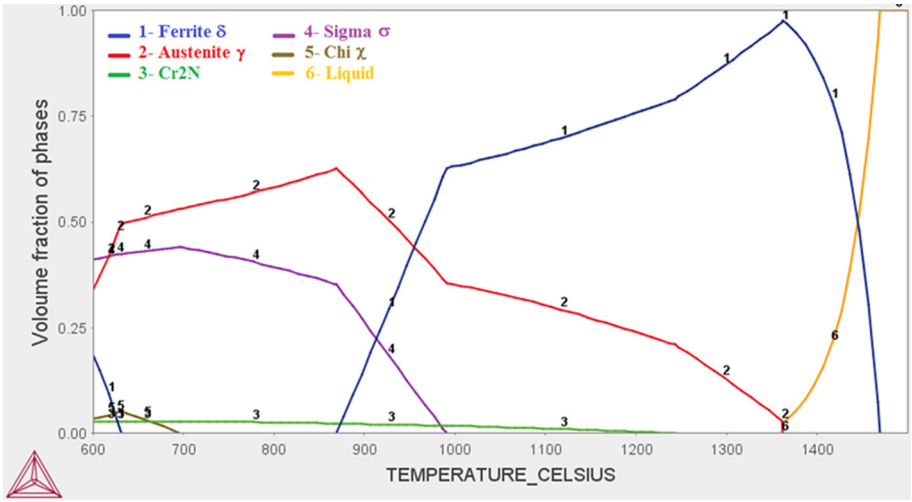

Fig. 4 Phase diagram of UNS S32750 calculated by Thermo-Calc software using TCFE7 database

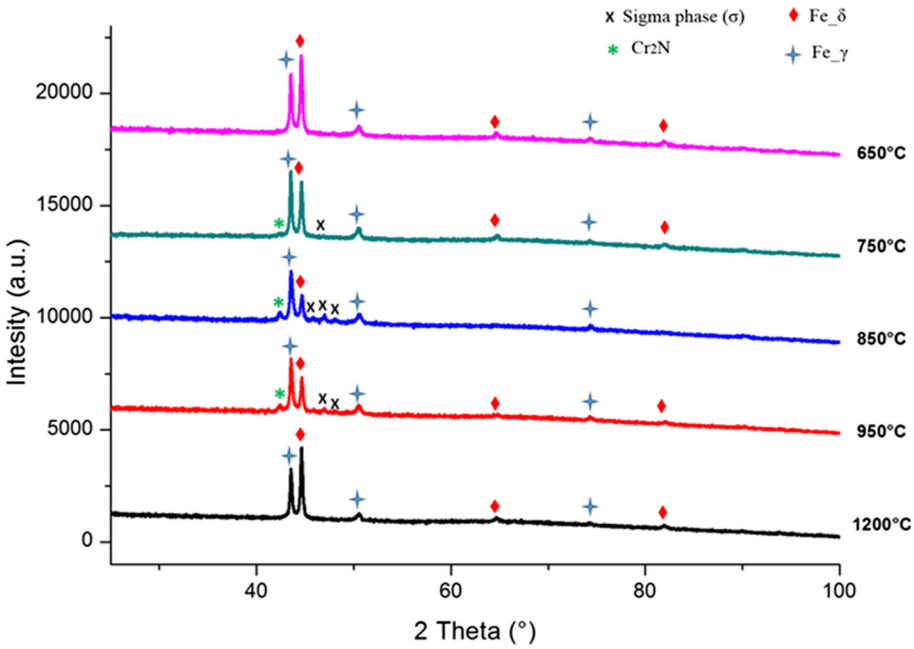

Fig. 5 X-ray diffractograms of the as-annealed and aged samples

mechanical properties (H_{IT} and E_{IT}) of the aged samples can easily be calculated as depicted in Fig. 6(b). The as-annealed and the sample aged at 650 °C exhibit roughly similar behavior with the lowest values of H_{IT} and E_{IT}. It can be seen that with increasing aging temperature, remarkable enhancement in the mechanical properties is obtained. The 850 °C aged sample has the highest hardness (6.7 GPa) and elastic modulus (247 GPa) due to the precipitation of high amount of σ phase and the presence of other hard compounds in microstructure such as Cr_2N. It is well documented that the hardness and the elastic modulus influence the mechanical properties as-well-as wear resistance (Ref 24, 25). Therefore, it is more suitable to consider both properties to predict the wear and mechanical behaviors of the studied material (Ref 20). In this study, the elastic strain to failure (H/E) so-called plasticity index, is measured to rank the aged samples according to their limit of elastic behavior to provide a close agreement in terms of wear resistance.

As seen in Table 4, the lowest plasticity index is recorded in the as-annealing condition (1200 °C) and after 650 °C aging treatment, where no apparent precipitates is observed as seen in Fig. 1(a) and (b). However, a clear tendency of increase in the plasticity index (H/E) with aging temperature up to 850 °C (30.6×10^{-3}) followed by a decrease with further aging temperature. The increase in mechanical properties especially at 850 and 950 °C is more probably attributed to the microstructure hardening as a result of σ and χ phase precipitation that enhance the surface resistance by increasing its plastic deformation during loading. Thereby, it is recommended to select these temperatures (750-950 °C) when hardness, and high elasto-plasticity properties as well as wear resistance (Ref 24) are the most important requirement.

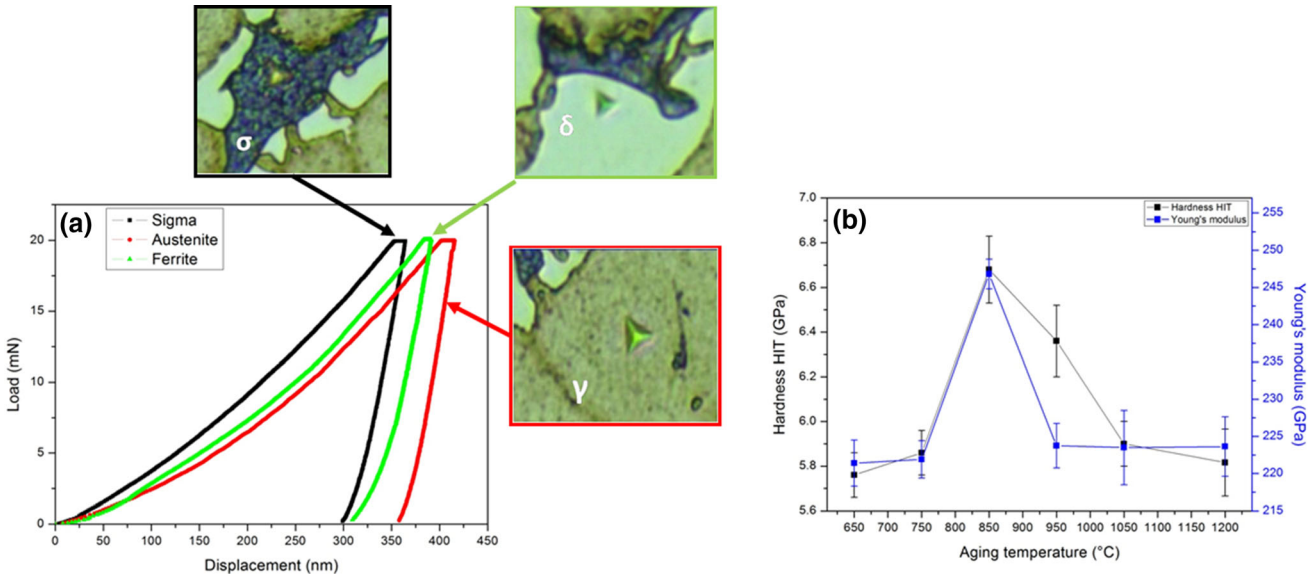

Fig. 6 Local mechanical properties of the aged samples: (a) load–displacement curves of different phases in the sample aged at 750 °C and (b) hardness (H_{IT}) and Young's modulus (E_{IT}) values as a function of aging temperature

Table 3 Hardness (H_{IT}) and Young's modulus (E_{IT}) measured in different phases of the 750 °C aged sample

	Ferrite (δ)	Austenite (γ)	Sigma phase (σ)
Hardness H_{IT}, GPa	6.6 ± 0.7	5.9 ± 0.5	8.8 ± 0.7
Young's modulus (E_{IT}), GPa	248 ± 2.1	238 ± 3.7	250 ± 4.2

Table 4 Plasticity index H/E measured in different aged samples

Aging temperature, °C	As-annealed	650	750	850	950	1050
H/E (10^{-3})	25.7 ± 0.5	26.8 ± 0.7	27.6 ± 0.6	30.6 ± 1.0	29.3 ± 0.6	27.6 ± 0.8

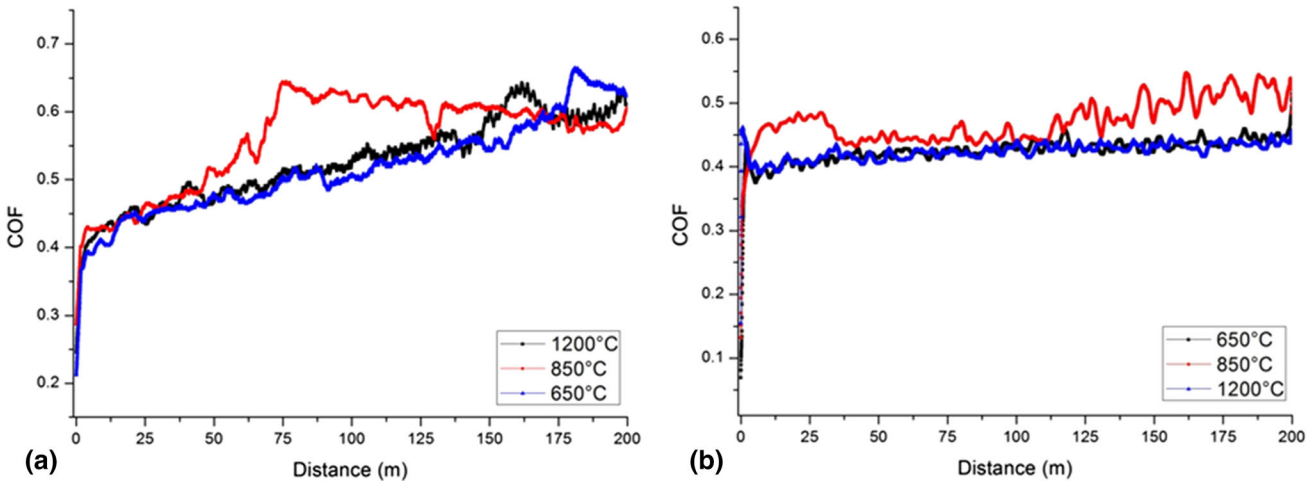

Fig. 7 Evolution of CoF with distance in samples aged at different temperatures under (a) Al_2O_3 counterpart and (b) AISI 304L counterpart

3.3 Tribological Behavior Under Different Conditions

Figure 7(a) and (b) shows the evolution of the coefficient of friction (CoF) with sliding distance for the samples aged at different temperatures against alumina (Al_2O_3) and AISI 304L counterparts, respectively. Each sample shows typical running-

in behavior against both counterparts where noises are present in data due to the vibration during the tests.

- Against Al_2O_3 counterpart

At the beginning of the test (Fig. 7a), the CoF of the as-annealed sample is 0.15 and increases rapidly to 0.52 after a short run-in-period where it stabilizes at this value during the first 100 m sliding distance. The CoF continues its increasing trend to 0.68 until the end of the test without reaching the steady state. The sample aged at 650 °C exhibits the same tendency with a continuous increasing in CoF to 0.69. However, dissimilar behavior is observed in the sample aged at 850 °C. The CoF increases and reaches its maximum value of 0.7 during the first 80 m run-in-period than it decreases slightly and stabilizes at 0.58 until the end of the test. The lowest CoF recorded in 850 °C aged sample is explained by the highest hardness induced by the precipitation of hard phases (discussed in section 3.1) that improves the surface resistance of the 2507 SDSS. This high hardness results in the decrease in sliding contact areas which consequently lower the frictional contact. Furthermore, the elastic interaction of Al_2O_3 ball with high Young's modulus obtained at 850 °C, reduces the CoF by increasing the effective elastic modulus (Ref 26). The similar microstructure features and roughly identical hardness values of the as-annealed and the sample aged at 650 °C (245HV and 260HV, respectively) suggest a similar friction behavior with high CoF. These results line with the findings of similar research works (Ref 1, 27, 28) Hence, it can be said that the better tribological behavior under Al_2O_3 counterpart is obtained at 850 °C aging temperature.

- Against AISI 304L counterpart

The plots of the CoF evolution of the aged samples against AISI 304L counterpart, are presented in Fig. 7(b). The as-annealed and 650 °C aged samples show a very similar tendency, both samples exhibit decreasing CoF values before reaching steady state after the first 10 m of sliding. This trend is more likely attributed to the fracturing of the surface and oxide layer (Fe_3O_4) (Ref 12) during the first short run-in period. As the debris are compacted, the CoF quickly reaches its steady state with low value (0.44 for both samples). The CoF trend suggests low adhesion forces in contact zones with more probably the formation of lubricant layer (Ref 1). The decreased hardness values in the as-annealed sample and the one aged at 650 °C promotes a high frictional contact, hence a lower CoF compared to the one obtained in 850 °C aged sample (0.52). Based on the CoF values, it can be said that the best combination sample/counterpart is obtained in the as-annealed and the 650 °C aged samples against AISI 304L ball, while against Al_2O_3 counterpart, the sample aged at 850 °C has the best tribological behavior.

The wear rates of the as-annealed and aged samples against alumina and AISI 304L counterparts are shown in Fig. 8. It is observed that, against both counterparts, the wear rates decrease with increasing aging temperature. It is found that the lowest values are recorded in the sample aged at 850 °C (3×10^{-14} and 5×10^{-14} mm^3/Nm against alumina and AISI 304L, respectively) then the wear rates increase to their maximum values (2.7×10^{-13} and 1.5×10^{-13} mm^3/Nm against alumina and AISI 304L, respectively) as approaching 1050 °C. The presence of high amount of σ phase, χ phase and Cr_2N in the

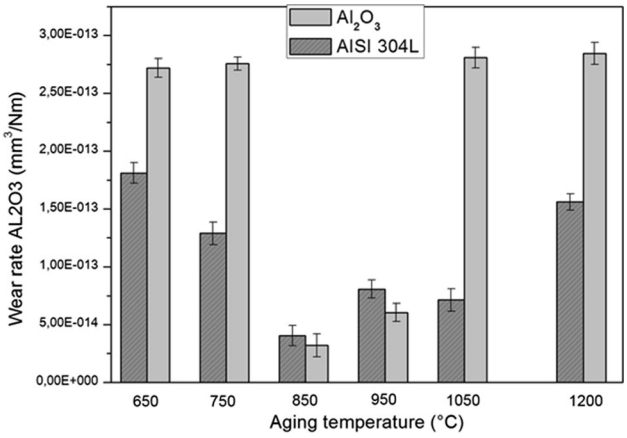

Fig. 8 Wear rate histograms of the as-annealed and aged samples obtained after tribology tests under Al_2O_3 and AISI 304L counterparts

microstructure of the aged samples promotes a better wear resistance. This behavior can be explained by the high hardness induced by σ phase precipitates that strengths the surface and improve its resistance against the stresses caused by the counterparts. Consequently, small amount of material is lost resulting from the low sensibility of material to shear and stress (Ref 9). As expected, the higher wear rates are recorded against alumina counterpart (roughly two times in the samples aged at 650 and 1050 °C). However, as the samples become harder (samples aged at 850 and 950 °C) the wear rates become lower, compared to the ones against AISI 304L counterparts which is in contrast to their CoF values. In order to elucidate the change in wear behavior of the aged samples against both counterparts, worn surfaces analyses are performed to understand the competition between the wear rate and CoF related to their microstructure and activated wear mechanisms.

The general aspect of the worn surfaces of the as-annealed sample against AISI 304L and alumina counterparts can be seen in Fig. 9(a) and (b), respectively. Both surfaces show similar surface damage, grooves and scratches are present that are more accentuated against alumina counterpart due to its high hardness. The wear tracks exhibit also adhesive mechanism and less debris against AISI 304L counterpart. EDS point analysis (A and B), conducted in the worn surfaces is summarized in Table 5. A significant amount of Al and O elements is detected in the surface worn against alumina counterpart, whereas only the steel elements with O are detected on the one against AISI 304 counterpart. The presence of O element and grooves suggest a combination of oxidative-abrasive wear mechanism against alumina counterpart, however, it is more adhesive under AISI 304L counterpart.

In the sample aged at 850 °C (Fig. 10a), the wear mechanism is less abrasive against Al_2O_3 counterpart due to the surface hardening and reduction in plastic deformation (high H/E ratio) Furthermore, the extent of oxides islands, (see spot C and D in Fig. 10b and c) are higher compared to ones against AISI 304L counterpart. The increase in temperature during the sliding test promotes the formation of tribofilm, more probably Fe_2O_3, which becomes increasingly brittle as the sliding increase, resulting in the breakup of the tribofilm into oxides islands (Ref 29). The worn surface of the sample aged at 850 °C against AISI 304L counterpart is shown in Fig. 11(a). Plowing mechanism is observed with a clear materials dis-

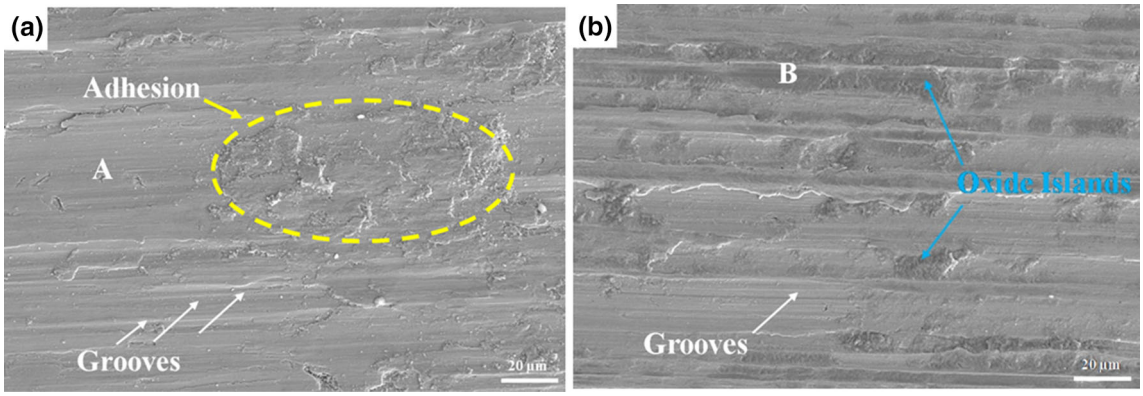

Fig. 9 SEM micrographs of the worn surfaces of the as-annealed sample: (a) against AISI 304L counterpart and (b) against Al_2O_3 counterpart

Table 5 EDS point analysis of the worn surfaces targeted in Fig. 9(b), 10(b), and 11(b) and (c)

Elements, wt.%	Fe	Ni	Cr	Mo	O	Al
A	61.4	4.7	24.1	2.3	4.2	…
B	53.6	5.6	17.6	1.9	14.8	6.5
C	44.8	4.5	19.8	2.1	22.3	8.5
D	35.6	3.9	18.3	1.1	25.4	15.7
E	58.4	6.8	21.6	1.6	13.2	…
F	64.2	6.5	24.8	2.7	1.8	…

placement outward from the wear track. It is known that this type of mechanisms does not generate an important material loss while a remarkable plastic deformation is involved. Vignal et al. (Ref 3) found that elastic straining of ferrite is generated during siding test with plastic deformation of austenite. On the other side, the sliding behavior of duplex stainless steel investigated by Shtraffelini et al. (Ref 30) revealed the formation of tribological layer and its fragmentation and detachment during sliding test. The high magnification of the worn surface shown in Fig. 11(b) exhibits deep grooves and microcracks induced by fatigue wear mechanism due to the shear-stress forces below the worn surface, which is responsible of the measured wear loss (Ref 29). It can be seen that the surface is covered by less dark islands reach in O and Ni that may constitute a compacted oxides which is confirmed by the EDS point analysis conducted in spot E and F (see Table 5). The high hardness of the phases induced from δ phase decomposition results in a brittle microstructure that during wear test and at high temperature generated by sliding may fragment to form with oxygen oxides (Fe_2O_3 and Fe_3O_4) which promotes to tribo-oxidation (Ref 12, 30).

In summary, the abrasive wear mechanism in the as-annealed sample against alumina is resulted in an increased wear rate with high CoF, where the low CoF recorded against AISI 304L is related to the adhesive wear mechanism. For the 850 °C aged samples, combination of adhesive/abrasive and oxidative wear mechanisms is obtained against alumina counterpart resulting in lower wear rate, while fatigue, abrasive and oxidative mechanisms against AISI 304L are responsible of the high wear rate and relatively low CoF.

4. Conclusion

In this work, microstructure characteristics of a USN S32750 super duplex stainless steel aged in the temperature range of 650-1050 °C was performed and correlated to their local mechanical properties and wear performances. The main conclusions can be drawn:

- The precipitation of σ phase and Cr_2N nitride is strongly affected by temperature. The increase in aging temperature results in increasing secondary phase's precipitation with higher dissolution of δ phase at 850 °C.
- The higher hardness and elastic modulus of σ phase played a key role in the macro-mechanical properties of the aged samples. The 850 °C aging temperature, with high σ phase content, resulted in higher hardness and Young's modulus with the best plasticity index, while the low mechanical properties were recorded in the as-annealed and 650 °C aged samples.
- Based on the CoF values, the best combination sample/counterpart was obtained in the as-annealed and the 650 °C aged samples against AISI 304L ball while with Al_2O_3 counterpart, 850 °C aged sample exhibited the best tribological behavior.
- Against both counterparts, the wear rates decreased with increasing aging temperature to 850 °C.
- Against alumina counterpart, abrasive wear mechanism in the as-annealed sample resulted in an increased wear rate with high CoF. However, the low CoF recorded against AISI 304L counterpart was related to the adhesive wear mechanism. On the other side, the high hardness of the 850 °C aged samples against alumina, resulted in an adhesive/abrasive and oxidative wear mechanisms with lower wear rate, while fatigue, abrasive and oxidative mechanisms against 304L were responsible for the high wear rate and relatively low CoF.

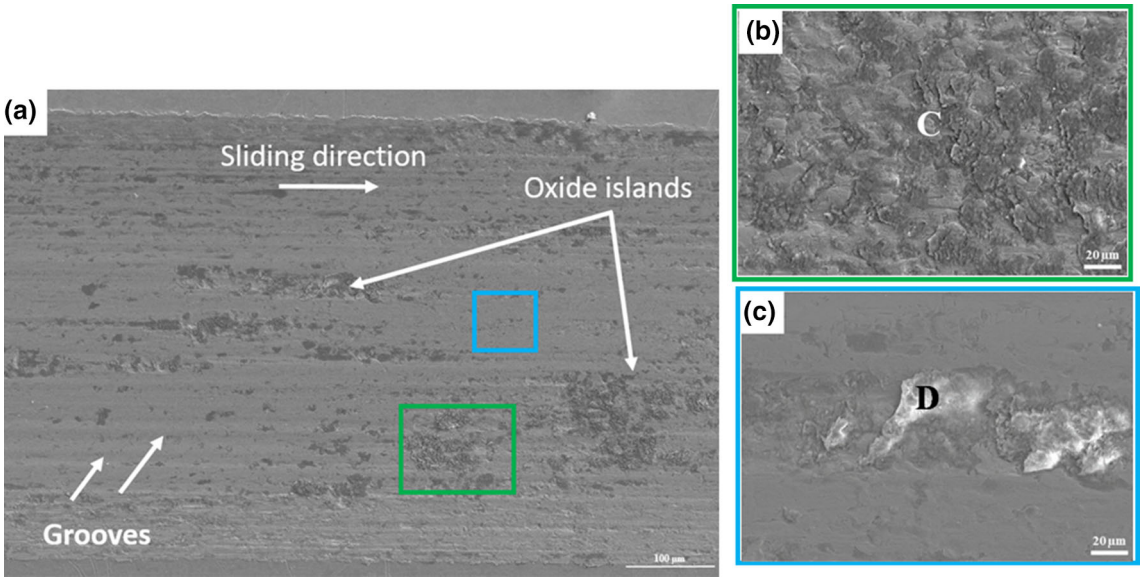

Fig. 10 SEM micrographs of the wear tracks of the sample aged at 850 °C: (a) against Al_2O_3 counterpart, (b) high magnification of oxide islands and (c) debris stacked on the worn surface

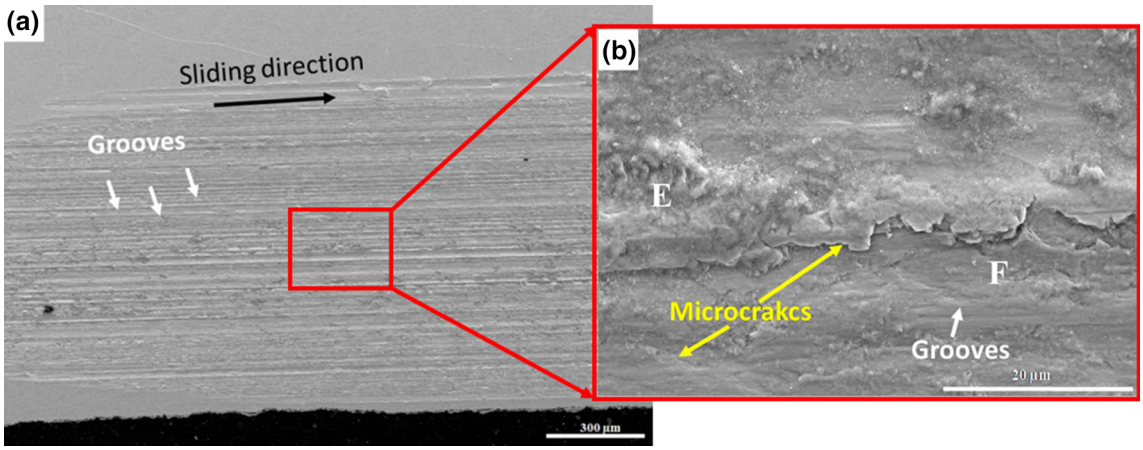

Fig. 11 SEM micrographs of the wear tracks of the sample aged at 850 °C. (a) Against AISI 304L counterpart and (b) high magnification of the worn surface

References

1. M. Davanageri, S. Narendranath, and R. Kadoli, Influence of Ageing Time on Hardness, Microstructure and Wear Behaviour of AISI2507 Super Duplex Stainless Steel, *Mater. Res. Express.*, 2007, **4**, p 086506
2. A.R. Akisanya, U. Obi, and N.C. Renton, Effect of Ageing on Phase Evolution and Mechanical Properties of a High Tungsten Super-Duplex Stainless Steel, *Mater. Sci. Eng., A*, 2012, **535**, p 281–289. https://doi.org/10.1016/j.msea.2011.12.087
3. B. Deng, Y.M. Jiang, J. Gao, and J. Li, Effect of Annealing Treatment on Microstructure Evolution and the Associated Corrosion Behavior of a Super-Duplex Stainless Steel, *J. Alloys Compd.*, 2010, **493**, p 461–464. https://doi.org/10.1016/j.jallcom.2009.12.127
4. M. Zhu, Q. Zhang, Y.F. Yuan, S.Y. Guo, and J. Pan, Passivation Behavior of 2507 Super Duplex Stainless Steel in Simulated Concrete Pore Solution, *J. Mater. Eng. Perform.*, 2020, https://doi.org/10.1007/s11665-020-04814-w
5. S. Steel, Effect of Sigma Phase Morphology on the Degradation Of Properties in a Super Duplex, *Materials*, 2018, https://doi.org/10.3390/ma11060933
6. H. Tan, Y. Jiang, B. Deng, T. Sun, J. Xu, and J. Li, Effect of Annealing Temperature on the Pitting Corrosion Resistance of Super Duplex Stainless Steel UNS S32750, *Mater. Charact.*, 2009, **60**, p 1049–1054. https://doi.org/10.1016/j.matchar.2009.04.009
7. J. Nilsson, Overview Super Duplex Stainless Steels, *Mater. Sci. Technol.*, 1992, **8**, p 685–700
8. B. Deng, Z. Wang, Y. Jiang, H. Wang, J. Gao, and J. Li, Evaluation of Localized Corrosion in Duplex Stainless Steel Aged at 850 °C with Critical Pitting Temperature Measurement, *Electrochim. Acta*, 2009, **54**, p 2790–2794. https://doi.org/10.1016/j.electacta.2008.11.038
9. M.B. Davanageri, S. Narendranath, and R. Kadoli, Influence of Heat Treatment on Microstructure, Hardness and Wear Behavior of Super Duplex Stainless Steel AISI, 2507, *Am. J. Mater. Sci.*, 2015, https://doi.org/10.5923/c.materials.201502.10
10. A. Laurent, M. Robin, M.A.G. Tommaselli, and C. Machado, Influence of the Solution-Treatment Temperature and Short Aging Times on the Electrochemical Corrosion Behaviour of Uns S32520 Super Duplex Stainless Steel, *Mater. Res.*, 2019, **22**, p 11–13
11. Z. Zhang, H. Zhang, J. Hu, X. Qi, Y. Bian, A. Shen, and P. Xu, Microstructure Evolution and Mechanical Properties of Briefly Heat-Treated SAF 2507 Super Duplex Stainless Steel Welds, *Constr. Build. Mater.*, 2018, **168**, p 338–345. https://doi.org/10.1016/j.conbuildmat.2018.02.143

12. M. Wang, Y. Wang, H. Liu, J. Wang, and F. Yan, Tribology International Interrelated Effects of Temperature and Load on Fretting Behavior of SAF 2507 Super Duplex Stainless Steel, *Tribiol. Int.*, 2019, **136**, p 140–147. https://doi.org/10.1016/j.triboint.2019.03.042
13. F. Marques, W.M. Silva, J.M. Pardal, S.S.M. Tavares, and C. Scandian, Influence of Heat Treatments on the Micro-abrasion Wear Resistance of a Superduplex Stainless Steel, *Wear*, 2011, **271**, p 1288–1294. https://doi.org/10.1016/j.wear.2010.12.087
14. G. Argandoña, J.F. Palacio, C. Berlanga, V. Biezma, and P.J. Rivero, Effect of the Temperature in the Mechanical Properties of Austenite, Ferrite and Sigma Phases of Duplex Stainless Steels Using Hardness, Microhardness and Nanoindentation Techniques, *Metals (Basel)*, 2017, https://doi.org/10.3390/met7060219
15. W.C. Oliver and G.M. Pharr, Measurement of Hardness and Elastic Modulus by Instrumented Indentation: Advances in Understanding and Refinements to Methodology, *J. Mater. Res.*, 2004, **19**, p 3–20. https://doi.org/10.1557/jmr.2004.19.1.3
16. K. Ravindranath, The Influence of Aging on the Intergranular Corrosion of 22 Chromium-5 Nickel Duplex Stainless Steel, *Corros. Sci.*, 1995, **37**, p 121–132
17. C. Science, P. Road, and O. Ox, U.K. Received, Metastable pitting in 14 Cr duplex stainless steel, (n.d.)
18. N. Sathirachinda, R. Pettersson, S. Wessman, U. Kivisäkk, and J. Pan, Scanning Kelvin Probe Force Microscopy Study of Chromium Nitrides in 2507 Super Duplex Stainless Steel —Implications and Limitations, *Electrochim. Acta*, 2011, **56**, p 1792–1798. https://doi.org/10.1016/j.electacta.2010.08.038
19. X. Jiang, T. Yoshimura, Y. Ishikawa, T. Shinoharo, and S. Tsujikawa, Investigation of Alpha Prime Precipitation in Aged Duplex Stainless Steel, *J. Electrochem. Soc.*, 1992, **139**, p 1001–1007
20. A. Leyland and A. Matthews, On the Significance of the H/E Ratio in Wear Control: A Nanocomposite Coating Approach to Optimised Tribological Behaviour, *Wear*, 2000, **246**, p 1–11
21. B. Yasuhiro, Precipitation of σ Phase in a 25Cr-7Ni-3Mo Duplex Phase Stainless Steel, *Trans. ISIJ*, 1983, **23**, p 240–246
22. M.E. Wilms, V.J. Gadgil, J.M. Krougman, B.H. Kolster, M.E. Wilms, V.J. Gadgll, J.M. Krougman, and B.H. Kolster, The Effect of σ-Phase Precipitation at 800°C on the Mechanical Properties of a High Alloyed Duplex Stainless Steel, *Mater. High Temp.*, 2016, https://doi.org/10.1080/09603409.1991.11689654
23. B. Cheniti, D. Miroud, R. Badji, P. Hvizdo, M. Fides, T. Csanádi, B. Belkessa, and M. Tata, Microstructure and Mechanical Behavior of Dissimilar AISI, 304L/WC-Co Cermet Rotary Friction Welds, *Mater. Sci. Eng., A*, 2019, **758**, p 36–46. https://doi.org/10.1016/j.msea.2019.04.081
24. T.L. Oberle, Properties Influencing Wear of Metals, *J. Met.*, 1951, **3**, p 438–439
25. U. Salford, S. Ms, and W.T. Gt, The Tribology of Surface Films, *Thin Solid Film*, 1983, **108**, p 103–115
26. T.B. Torgerson, M.D. Harris, S.A. Alidokht, T.W. Scharf, S.M. Aouadi, R.R. Chromik, J.S. Zabinski, and A.A. Voevodin, Room and Elevated Temperature Sliding Wear Behavior of Cold Sprayed Ni-WC Composite Coatings, *Surf. Coat. Technol.*, 2018, **5**, p 3. https://doi.org/10.1016/j.surfcoat.2018.05.090
27. J.M. Shockley, D.J. Horton, and J. Kathryn, Author' s Accepted Manuscript, *Wear*, 2017, https://doi.org/10.1016/j.wear.2017.03.019
28. F. Engineering, Dry Sliding Wear Behavior of Super Duplex Stainless Steel AISI, 2507: A Statistical Approach, *Arch. Found. Eng.*, 2016, **16**, p 47–56. https://doi.org/10.1515/afe
29. A. Mestra, G. Fargas, M. Anglada, and A. Mateo, Sliding Wear Behavior of a Duplex Stainless Steel, *Key Eng. Mater.*, 2010, **423**, p 125–130. https://doi.org/10.4028/www.scientific.net/KEM.423.125
30. G. Straffelini, D. Trabucco, and A. Molinari, Sliding Wear of Austenitic and Austenitic-Ferritic Stainless Steels, *Metall. Mater. Trans. A*, 2002, **33**, p 613–624